Cubic Phase Formation and Interplay between Alkyl Chains and Hydrogen Bonds in 1,2-Bis(4′-*n*-alkoxybenzoyl)hydrazines (BABH-*n*)

Shoichi Kutsumizu,*,† Hiroyuki Mori,† Machiko Fukatami,† Shigeharu Naito,† Koichi Sakajiri,† and Kazuya Saito‡

Department of Chemistry, Faculty of Engineering, Gifu University, 1-1 Yanagido, Gifu 501-1193, Japan, and Department of Chemistry, Graduate School of Pure and Applied Sciences, University of Tsukuba, Tsukuba, Ibaraki 305-8571, Japan

Received December 26, 2007. Revised Manuscript Received February 16, 2008

The phase transitions of a homologous series of 1,2-bis(4′-*n*-alkoxybenzoyl)hydrazines (BABH-*n*, where *n* is the number of carbon atoms in the alkyl chain and in this investigation varies from 4 to 22) were investigated by differential scanning calorimetric (DSC), polarizing optical microscopic (POM), X-ray diffraction (XRD), and infrared (FT-IR) measurements. The formation of bicontinuous type cubic (Cub) mesophases was observed enantiotropically for $n \geq 6$ and only on cooling for $n = 5$. The structures were examined by XRD, which revealed the presence of two types with symmetries *Ia*3*d* and *Im*3*m*, depending on *n*, and for $n = 13$, 15, and 16, phase transitions between the two Cub phases were observed. The FT-IR studies elucidated the formation of intermolecular hydrogen bonding between the C═O bond of one molecule and the NH group of another molecule, whose binding strength was temperature-dependent. The temperature dependence of the Cub lattice parameter (d*a*/d*T*) varied from a large positive to a large negative value with increasing alkyl chain length *n*, which can be well-explained in terms of the temperature-responsive shape change of the constituent molecules. The packing structures of two *Ia*3*d*-Cub phases formed by shorter and longer alkyl chain members are compared and discussed. It is revealed that two competitive mechanisms are mainly operated on the self-organization, i.e., the preferential orientation of the long axes of the aromatic core parts parallel to each other and microsegregation between the aromatic core and alkyl chain parts of the molecules; the former mechanism is effective in the shorter chain members, whereas the latter is predominant in the longer chain members.

Introduction

Thermotropic cubic (Cub) mesophases, especially bicontinuous types, are very mysterious in that both liquidlike molecular state and three-dimensionally long-range periodicity are realized in them.[1–6] The most often observed structure has a cubic symmetry *Ia*3*d*, which consists of two pairs of 3-by-3 interpenetrating networks.[7,8] If connecting all the midway points between the two networks, one obtains the so-called triply periodic minimal surface (TPMS) of type G, alternatively called gyroid; in the ideal situation, the portion of the TPMS is a saddle surface with zero mean curvature and negative Gaussian curvature.[9,10] The structure is one of the most complicated in liquid crystals (LCs). Because many other compatible TPMSs are known in mathematics,[9] why nature prefers the *Ia*3*d*-gyroid phase still remain unanswered completely. Thus, the Cub phases have attracted great attention not only in the thermotropic LCs but in the more broad area of soft matter science.

Qualitatively, the formation of the *Ia*3*d*-gyroid phase is understood as a result of microphase separation between two chemically incompatible components (e.g., hydrophilic vs hydrophobic or aliphatic vs aromatic) and of packing frustration arising from parallel surfaces of the two components when the volume ratio is deviated from 1:1.[2–6] Such understanding basically comes from the analogy of lyotropic Cub systems, but when considering the packing structure, another problem arises. Because the unit lattice contains hundreds of or thousands of molecules, it is not easy to determine the packing structure only from the lattice dimension and symmetry. In the lyotropic systems, it can be presumed that the space between the curved TPMSs decorated by one component is filled by the other not covalently

* To whom correspondence should be addressed. E-mail: kutsu@gifu-u.ac.jp.
† Gifu University.
‡ University of Tsukuba.

(1) Gray, G. W.; Goodby, J. W. In *Smectic Liquid Crystals, Textures and Structure*; Leonard Hill: Glasgow, U.K., 1984; pp 68−81, including earlier references on thermotropic cubic phases.
(2) Diele, S.; Göring, P. In *Handbook of Liquid Crystals*; Demus, D., Goodby, J., Gray, G. W., Spiess, H.-W., Vill, V., Eds.; Wiley-VCH: Weinheim, Germany, 1998; Vol. 2B, pp 887−900.
(3) Tschierske, C. *Annu. Rep. Prog. Chem., Sect. C* **2001**, *97*, 191–267, and references therein.
(4) Diele, S. *Curr. Opin. Colloid Interface Sci.* **2002**, *7*, 333–342.
(5) Kutsumizu, S. *Curr. Opin. Solid State Mater. Sci.* **2002**, *6*, 537–543.
(6) Impéror-Clerc, M. *Curr. Opin. Colloid Interface Sci.* **2005**, *9*, 370–376.
(7) Schoen, A. H. *Infinite Periodic Minimal Surfaces without Self-Intersections*; NASA Technical Note D-5541; National Aeronautics and Space Administration: Washington, D.C., 1970; pp 1−92.
(8) Luzzati, V.; Spegt, P. A. *Nature* **1967**, *215*, 701–704.
(9) Hyde, S.; Andersson, S.; Larsson, K.; Blum, Z.; Landh, T.; Lidin S.; Ninham, B. W. *The Language of Shape, The Role of Curvature in Condensed Matter: Physics, Chemistry and Biology*; Elsevier: Amsterdam, 1997.
(10) *Bicontinuous Liquid Crystals*; Lynch, M. L., Spicer, P. T., Eds.; Surfactant Science Series; CRC Press: Boca Raton, FL, 2005; Vol. 127.

10.1021/cm703684v CCC: $40.75
Published on Web 04/26/2008

bonded to the former. However, most of the thermotropic Cub phases are formed by one kind of constituent molecules, which implies that when viewed microscopically, all the molecules are in the same environment, at least if time-averaged, by taking translational diffusion of the molecules into consideration. Therefore, the situation is more complicated than that in lyotropic systems. At the present stage, understanding of the packing structure in the thermotropic Cub phases is far from complete.

As aforementioned, most often observed Cub structure is *Ia*3*d*-gyroid type, but in lyotropic systems, a few examples were reported having structures described by P- and D-type TPMSs, which are compatible with cubic symmetries *Im*3*m* and *Pn*3*m*, respectively.[10,11] Several examples in thermotropic systems also have cubic symmetries *Im*3*m*[12] and *Pn*3*m*,[13] but the former cases are all not consistent with a structure described by the above P-type TPMS. For this problem, Levelut and Clerc[14] proposed a Cub lattice containing three continuous surfaces, where in addition to the usual P-type, two parallel surfaces are added in both sides. Unfortunately, this was not the final answer, because in this model, space surrounded by two neighboring surfaces is too small at some locations compared to the molecular size. Here, it should be noted that the *Im*3*m* structure is restricted to thermotropic systems only, not seen in other systems such as lyotropics or block copolymers.

To date, the number of examples exhibiting thermotropic Cub phases has greatly increased: carboxylic acids,[15] chiral and achiral hydrazines,[16] chiral pyrimidine,[17] lipids,[8,18] metal mesogens,[19] polyols,[20] siloxanes,[21] biforked mesogens,[12a,22] coil−rod−coil molecules,[23] ionic polymers,[13a,24] etc. Nevertheless, there is no molecular design principle for forming thermotropic Cub phases. In this respect, our knowledge is still very fragmented, especially regarding chemical structures (the number and length of aliphatic chain(s), and the position connected to the core, core size, etc.). Our ultimate goal is to fully understand how each chemical part contributes to the formation of the Cub phase when temperature is changed. For this purpose, we felt the necessity of a systematic research with respect to the chemical structure, and our first selection was 4′-*n*-alkoxy-3′-nitrobiphenyl-4-carboxylic acid (ANBC-*n*) series.[25] The compounds were first synthesized by Gray and co-workers[15a] and a representative Cub phase forming compound at that time.[15] Since lengthening the alkyl chain changes the volume fraction of this part in the system in analogy with the case of lyotropic LC systems, such investigation was expected to clarify the influence of the chain length on the mesophase formation and also to reveal some differences between the two LC systems.

In fact, exploring the Cub phase forming members in the same series provided us many fruitful results.[26–36] On the basis of the data on the SmC-to-Cub phase transition entropy dependent on the alkyl chain length, an important role of the chain part during the formation of the Cub phase in competition with the layered SmC phase was elucidated; in the Cub phase, the chain part is more disordered, whereas the core part is more ordered than in the SmC phase ("alkyl chain as an entropy reservoir" mechanism).[26] The region of the Cub phase contains two types of structure, the *Ia*3*d*-gyroid and *Im*3*m* phases,[27,28] which led to elucidation of the structure of the latter *Im*3*m* phase (doubled P TPMS (PP-TPMS) model);[5,26d,28] as its modified version, a more sophisticated model was recently presented by Zeng et al.[29] The PP-TPMS model itself was first introduced by Góźdź and Hołyst.[37] The Cub phase exhibits a relatively high elasticity compared with other LC phases of the same compound, reflecting the bicontinuity of the structure;[30] for this reason, the Cub phase is classified into a category of materials soft crystals.[31] The heat capacity measurements demonstrated the reduction of thermal fluctuation in the Cub phase, also attributable to the bicontinuity.[26b,32] These two facts are in striking contrast with their microscopic state almost comparable to the isotropic liquid state, which was evidenced by using infrared (IR)[33] and nuclear magnetic

(11) (a) Longley, W.; McIntosh, T. J. *Nature* **1983**, *303*, 612–613. (b) Larsson, K. *Nature* **1983**, *304*, 664. (c) Hyde, S. T.; Andersson, S.; Ericsson, B.; Larsson, K. A. *Z. Kristallogr.* **1984**, *168*, 213–219.

(12) (a) *Im*3*m* first paper: Nguyen, H. T.; Destrade, C.; Levelut, A.-M.; Malthête, J. *J. Phys. (Paris)* **1986**, *47*, 553–557. (b) Levelut, A.-M.; Fang, Y. *Colloq. Phys.* **1990**, *51*, C7−229C7−236.

(13) (a) Thermotropic *Pn*3*m* first paper: Ujiie, S.; Mori, A. *Mol. Cryst. Liq. Cryst.* **2005**, *437*, 25–31. (b) Ichihara, M.; Suzuki, A.; Hatsusaka, K.; Ohta, K. *Liq. Cryst.* **2007**, *34*, 555–567.

(14) Levelut, A.-M.; Clerc, M. *Liq. Cryst.* **1998**, *24*, 105–115.

(15) (a) Gray, G. W.; Jones, B.; Marson, F. *J. Chem. Soc.* **1957**, 393–401. (b) Demus, D.; Kunicke, G.; Neelsen, J.; Sackmann, H. *Z. Naturforsch., A* **1968**, *23*, 84–90. (c) Pelzl, G.; Sackmann, H. *Symp. Chem. Soc., Faraday Discuss.* **1971**, *5*, 68–96. (d) Tardieu, A.; Billard, J. *J. Phys. (Paris) Colloq.* **1976**, *C3* (37), 79–81. (e) Demus, D.; Marzotko, D.; Sharma, N. K.; Wiegeleben, A. *Krist. Tech.* **1980**, *15*, 331–339. (f) Gray, G. W. *Zehn Arbeiten über Flüssige Kristalle*; Kongress-und Tagungs-berichte der Martin-Luther-Universität: Halle-Wittenberg, 1986; pp 22−42.

(16) (a) Schubert, H.; Hauschild, J.; Demus, D.; Hoffmann, S. *Z. Chem.* **1978**, *18*, 256. (b) Demus, D.; Gloza, A.; Hartung, H.; Hauser, A.; Rapthel, I.; Wiegeleben, A. *Cryst. Res. Technol.* **1981**, *16*, 1445–1451. (c) Göring, P.; Diele, S.; Fischer, S.; Wiegeleben, A.; Pelzl, G.; Stegemeyer, H.; Thyen, W. *Liq. Cryst.* **1998**, *25*, 467–474.

(17) (a) Yoshizawa, A.; Umezawa, J.; Ise, N.; Sato, R.; Soeda, Y.; Kusumoto, T.; Sato, K.; Hiyama, T.; Takanishi, Y.; Takezoe, H. *Jpn. J. Appl. Phys.* **1998**, *37*, L942–L944. (b) Takanishi, Y.; Ogasawara, T.; Yoshizawa, A.; Umezawa, J.; Kusumoto, T.; Hiyama, T.; Ishikawa, K.; Takezoe, H. *J. Mater. Chem.* **2002**, *12*, 1325–1330.

(18) (a) Luzzati, V.; Mustacchi, H.; Skoulios, A. *Faraday Discuss.* **1958**, *25*, 43–50. (b) Mariani, P.; Luzzati, V.; Delacroix, H. *J. Mol. Biol.* **1988**, *204*, 165–189.

(19) (a) Bruce, D. W.; Dummur, D. A.; Hudson, S. A.; Lalinde, E.; Maitlis, P. M.; McDonald, M. P.; Orr, R.; Styring, P. *Mol. Cryst. Liq. Cryst.* **1991**, *206*, 79–92. (b) Bruce, D. W. *Acc. Chem. Res.* **2000**, *33*, 831–840. (c) Hatsusaka, K.; Ohta, K.; Yamamoto, I.; Shirai, H. *J. Mater. Chem.* **2001**, *11*, 423–433. (d) Hatsusaka, K.; Kimura, M.; Ohta, K. *Bull. Chem. Soc. Jpn.* **2003**, *76*, 781–787. (e) Neve, F.; Clerc, M. *Liq. Cryst.* **2004**, *31*, 907–912. (f) Massiot, P.; Impéror-Clerc, M.; Veber, M.; Deschenaux, R. *Chem. Mater.* **2005**, *17*, 1946–1951.

(20) (a) Borisch, K.; Diele, S.; Göring, P.; Tschierske, C. *Chem. Commun.* **1996**, 237–238. (b) Borisch, K.; Diele, S.; Göring, P.; Müller, H.; Tschierske, C. *Liq. Cryst.* **1997**, *22*, 427–443.

(21) (a) Nishikawa, E.; Samulski, E. T. *Liq. Cryst.* **2000**, *27*, 1457–1462. (b) Nishikawa, E.; Samulski, E. T. *Liq. Cryst.* **2000**, *27*, 1463–1471.

(22) Nguyen, H.-T.; Destrade, C.; Malthête, J. In *Handbook of Liquid Crystals*; Demus, D., Goodby, J., Gray, G. W., Spiess, H.-W., Vill, V., Eds.; Wiley-VCH: Weinheim, Germany, 1998; Vol. 2B, pp 865–885.

(23) (a) Lee, M.; Cho, B.-K.; Kim, H.; Yoon, J.-Y.; Zin, W.-C. *J. Am. Chem. Soc.* **1998**, *120*, 9168–9179. (b) Lee, M.; Yoo, Y.-S. *J. Mater. Chem.* **2002**, *12*, 2161–2168.

(24) Tsiourvas, D.; Paleos, C. M.; Skoulios, A. *Macromolecules* **1999**, *32*, 8059–8065.

(25) Kutsumizu, S.; Yamada, M.; Yano, S. *Liq. Cryst.* **1994**, *16*, 1109–1113.

Scheme 1. Preparation Route of BABH-*n*

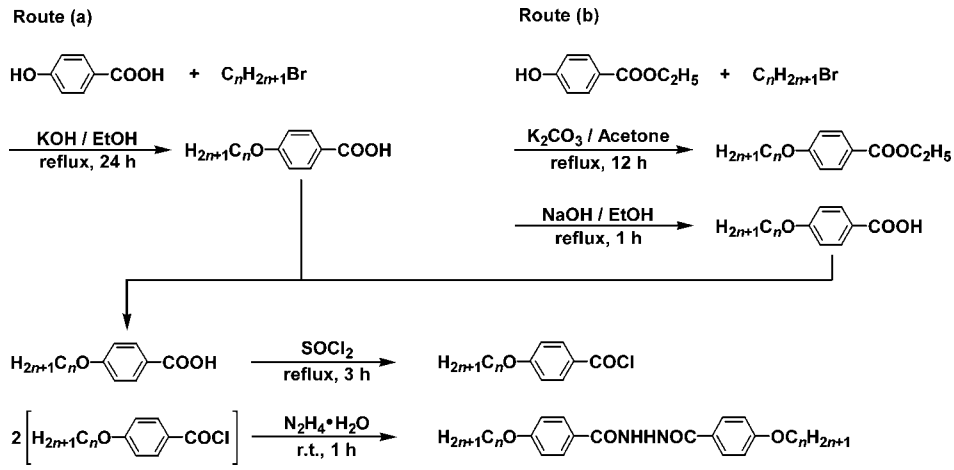

resonance (NMR)[34] spectroscopies. Thus, the ANBC-*n* series are now one of the most characterized Cub phase forming systems.

To gain generalized design principles, we moved our target to 1,2-bis(4′-*n*-alkoxybenzoyl)hydrazines (BABH-*n*) system,[32a,38] for which only few reports were known.[15] In the ANBC-*n* system, hydrogen-bonded dimers are the basic units constructing the self-organized structures,[33] and the chemical structures of the two systems BABH-*n* and ANBC-*n* are similar in that they are composed of a rigid aromatic core at the center and a flexible alkyl tail at each end. On the one hand, a difference between the two is that hydrogen bonding in the BABH-*n* system is intermolecular interactions acting laterally with respect to the molecular long axis.[39] Another is that the SmC phase is always at the low temperature side of the Cub phase region in the ANBC-*n* system[25] whereas at the high temperature side and limited only for $n = 8-10$ in the BABH-*n* system.[16b] Our preliminary communication[40] with respect to *n* revealed that the Cub phase region of the BABH-*n* system also contains both *Ia*3*d*-gyroid and *Im*3*m* phases and this fact motivated us to investigate this system in more detail.

In this paper, we first report the complete phase diagram of BABH-*n*. In the diagram, we note the presence of Cub-to-Cub phase transitions for three members. On the basis of the data obtained from combined techniques of X-ray diffraction (XRD) and Fourier transform infrared (FT-IR) spectroscopy, we then discuss and clarify the relationship between the self-organized structures of the Cub phases and temperature-responsive shape change of the constituent molecules. Finally, we compare the molecular packing structures of two *Ia*3*d*-gyroid phase regions divided by the *Im*3*m* phase region and discuss the differences observed and their origins.

Experimental Section

Preparation. Preparation route of BABH-*n* is outlined in Scheme 1, which is essentially the same as reported by Schubert et al.[16a] but slightly modified to improve the purity and/or to obtain longer alkyl chain homologues. The first step is Williamson etherification of either 4-hydroxybenzoic acid (in route a) or ethyl 4-hydroxybenzoate (in route b) to obtain the corresponding 4-*n*-alkoxy compound; in the latter route, saponification gave the same product

(26) (a) Saito, K.; Sato, A.; Sorai, M. *Liq. Cryst.* **1998**, *25*, 525–530. (b) Sato, A.; Yamamura, Y.; Saito, K.; Sorai, M. *Liq. Cryst.* **1999**, *26*, 1185–1195. (c) Saito, K.; Shinhara, T.; Sorai, M. *Liq. Cryst.* **2000**, *27*, 1555–1559. (d) Saito, K.; Sorai, M. *Chem. Phys. Lett.* **2002**, *366*, 56–61. (e) Sorai, M.; Saito, K. *Chem. Rec.* **2003**, *3*, 29–39.
(27) (a) Kutsumizu, S.; Ichikawa, T.; Nojima, S.; Yano, S. *Chem. Commun.* **1999**, 1181–1182. (b) Kutsumizu, S.; Kobayashi, H.; Nakamura, N.; Ichikawa, T.; Yano, S.; Nojima, S. *Mol. Cryst. Liq. Cryst.* **2000**, *347*, 239–248. (c) Kutsumizu, S.; Ichikawa, T.; Yamada, M.; Nojima, S.; Yano, S. *J. Phys. Chem., B* **2000**, *44*, 10196–10205. (d) Kutsumizu, S.; Morita, K.; Ichikawa, T.; Yano, S.; Nojima, S.; Yamaguchi, T. *Liq. Cryst.* **2002**, *29*, 1447–1458.
(28) Kutsumizu, S.; Morita, K.; Yano, S.; Nojima, S. *Liq. Cryst.* **2002**, *29*, 1459–1468.
(29) Zeng, X.; Ungar, G.; Impéror-Clerc, M. *Nat. Mater.* **2005**, *4*, 562–567.
(30) (a) Yamaguchi, T.; Yamada, M.; Kutsumizu, S.; Yano, S. *Chem. Phys. Lett.* **1995**, *240*, 105–108. (b) Kutsumizu, S.; Yamaguchi, T.; Kato, R.; Yano, S. *Liq. Cryst.* **1999**, *26*, 567–573. (c) Kutsumizu, S.; Yamaguchi, T.; Kato, R.; Ichikawa, T.; Yano, S. *Mol. Cryst. Liq. Cryst.* **1999**, *330*, 359–365. (d) Kutsumizu, S.; Yamada, M.; Yamaguchi, T.; Tanaka, K.; Akiyama, R. *J. Am. Chem. Soc.* **2003**, *125*, 2858–2859. (e) Tanaka, K.; Akiyama, R.; Takano, M.; Kutsumizu, S.; Yamaguchi, T. *Trans. Mater. Res. Soc. Jpn.* **2004**, *29*, 815–818.
(31) (a) Nozières, P.; Pistolesi, F.; Balibar, S. *Eur. Phys. J. B* **2001**, *24*, 387–394. (b) Even, C.; Impéror-Clerc, M.; Pieranski, P. *Eur. Phys. J. E* **2006**, *20*, 89–98.
(32) (a) Morimoto, N.; Saito, K.; Morita, Y.; Nakasuji, K.; Sorai, M. *Liq. Cryst.* **1999**, *26*, 219–228. (b) Sato, A.; Saito, K.; Sorai, M. *Liq. Cryst.* **1999**, *26*, 341–349. (c) Saito, K.; Shinhara, T.; Nakamoto, T.; Kutsumizu, S.; Yano, S.; Sorai, M. *Phys. Rev. E* **2002**, *65*, 031719.
(33) Kutsumizu, S.; Kato, R.; Yamada, M.; Yano, S. *J. Phys. Chem., B* **1997**, *101*, 10666–10673.
(34) (a) Ukleja, P.; Siatkowski, R. E.; Neubert, M. E. *Phys. Rev. A* **1988**, *38*, 4815–4821. (b) Tansho, M.; Onoda, Y.; Kato, R.; Kutsumizu, S.; Yano, S. *Liq. Cryst.* **1998**, *24*, 525–529.
(35) (a) Impéror-Clerc, M.; Sotta, P.; Veber, M. *Liq. Cryst.* **2000**, *27*, 1001–1009. (b) Impéror-Clerc, M.; Veber, M.; Levelut, A.-M. *ChemPhysChem* **2001**, 533–535.
(36) (a) Shankar Rao, D. S.; Prasad, S. K.; Prasad, V.; Kumar, S. *Phys. Rev. E* **1999**, *59*, 5572–5576. (b) Maeda, Y.; Cheng, G.-P.; Kutsumizu, S.; Yano, S. *Liq. Cryst.* **2001**, *28*, 1785–1791. (c) Maeda, Y.; Prasad, S. K.; Kutsumizu, S.; Yano, S. *Liq. Cryst.* **2003**, *30*, 7–16. (d) Maeda, Y.; Morita, K.; Kutsumizu, S. *Liq. Cryst.* **2003**, *30*, 157–164. (e) Kutsumizu, S.; Yamada, M.; Yano, S.; Tadano, K.; Nojima, S.; Yamaguchi, T. *Mol. Cryst. Liq. Cryst.* **2004**, *412*, 49–58.
(37) Góźdź, W. T.; Hołyst, R. *Phys. Rev. E* **1996**, *54*, 5012–5027.
(38) (a) Maeda, Y.; Ito, T.; Kutsumizu, S. *Liq. Cryst.* **2004**, *31*, 623–632. (b) Maeda, Y.; Ito, T.; Kutsumizu, S. *Liq. Cryst.* **2004**, *31*, 807–820. (c) Maeda, Y.; Ito, T.; Kutsumizu, S.; Saito, K.; Sorai, M. *Mol. Cryst. Liq. Cryst.* **2005**, *436*, 177–201.
(39) (a) Yoneya, M.; Nishikawa, E.; Yokoyama, H. *J. Chem. Phys.* **2002**, *116*, 5753–5758. (b) Yoneya, M.; Nishikawa, E.; Yokoyama, H. *J. Chem. Phys.* **2004**, *120*, 3699–3705.
(40) (a) Mori, H.; Kutsumizu, S.; Ito, T.; Fukatami, M.; Saito, K.; Sakajiri, K.; Moriya, K. *Chem. Lett.* **2006**, *35*, 362–363. (b) Kutsumizu, S.; Mori, H.; Fukatami, M.; Saito, K. *J. Appl. Crystallogr.* **2007**, *40*, s279–s282.

obtained in the former with higher yield and purity. The next step contains transformation of 4-*n*-alkoxy benzoic acid into the acid chloride, followed by a reaction with hydrazine monohydrate, to give the final product BABH-*n*. The crude product was recrystallized from adequate solvents and dried under a vacuum. The purity of all intermediary and final compounds was checked by a combination of thin-layer chromatography (TLC), NMR spectroscopy, and elemental analysis, and those data together with the detail preparation procedures are compiled in the Supporting Information.

Measurements. ^{1}H NMR (400 MHz) spectra were recorded on a JEOL JNM-α400 spectrometer, and $CDCl_3$ or C_6D_6 was used as solvent and tetramethylsilane as internal standard.

Phase transitions were examined using a Seiko Denshi DSC-210 interfaced to a TA data station (SSC 5000 system). The measurements were performed under a dry N_2 flow of ~40 mL min^{-1} and the scanning rate was 5 K min^{-1}. The texture of each mesophase was observed using a Nikon Optiphot-pol XTP-11 polarizing optical microscope (POM) equipped with a Mettler FP82 hot stage and a Mettler FP80 central processor at a heating/cooling rate of 5 K min^{-1}.

X-ray diffraction (XRD) patterns at elevated temperatures were obtained for powder samples. Two setups were used. The first setup was a Rigaku NANO-Viewer IP system, which was operated with a copper target at 45 kV and 60 mA. The scattered X-rays were recorded on a two-dimensional imaging plate (IP). The intensities were radially integrated and averaged, and redistributed when converting the pixel number into the corresponding scattering vector q ($q = (4\pi/\lambda)\sin\theta$, with λ being the X-rays wavelength (= 0.15418 nm) and 2θ the scattering angle) to produce a circularly averaged pattern. The second setup is the small-angle X-ray scattering equipment for solutions (SAXES) developed by Ueki et al.[41] and installed on beamline BL-10C at the Photon Factory (PF), Institute of Materials Structure Sciences, High Energy Accelerator Research Organization (KEK), Tsukuba, Japan, which uses synchrotron radiation as the X-ray source (λ = 0.1488 nm). The scattered intensity was detected by a linear position-sensitive proportional counter (PSPC). In the first setup, the IP recording is unable to avoid some uncertainty concerning the position of the direct beam ($q = 0$); the IP film must be detached from the optics to read the pattern at each temperature during the measurements. To determine the precise temperature variation of the lattice parameter for BABH-12, we had to use the second setup.

IR spectra were recorded with a Perkin-Elmer system 2000 Fourier transform IR spectrometer for the samples dispersed in KBr pellets.

The detailed procedures of the DSC, POM, XRD, and IR measurements are described in the Supporting Information.

Results

DSC Thermograms. Figure 1 displays differential scanning calorimetric (DSC) thermograms of BABH-*n* members recorded on the second heating scan (scanning rate: 5 K min^{-1}); for the $n = 5$ member, the first cooling scan is also shown. The Cub phase was detected enantiotropically for all members with $n \geq 6$ and only on cooling for the $n = 5$ member. The formation of the Cub phase was easily evidenced by polarized optical microscopic (POM) observation as the completely black texture[15b,e] was observed under crossed polarizers, which was further confirmed by X-ray diffraction (XRD) method. Although in agreement with the previous report by Demus et al.,[16b] for the $n = 8-10$ members, another mesophase, a smectic C (SmC) phase was detected at the high temperature side of the Cub phase on both heating and cooling, which was characterized by a typical SmC schlieren texture when viewed by POM. In addition, the members with $n = 4$, 6−15 have two or three crystalline states. The identification of those crystalline states was very difficult to accomplish but on the basis of the data on transition enthalpies and XRD profiles we attempted to classify them using the suffix (*m*) (see also the Supporting Information, Figure S0); as for the Cr_1 and Cr_1' phases, the XRD patterns were unable to distinguish them. All the DSC parameters are compiled in the Supporting Information, Table S1.

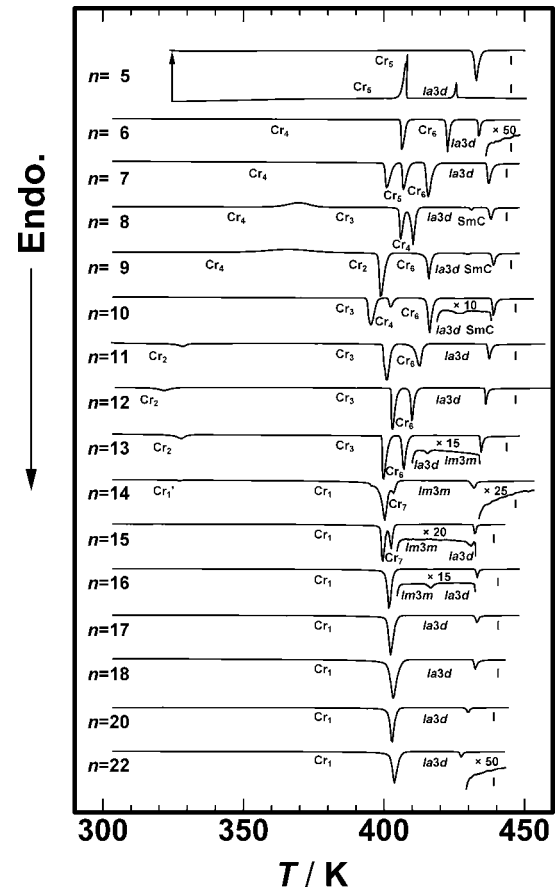

Figure 1. DSC thermograms of BABH-*n* members recorded on the second heating scan (scanning rate: 5 K min^{-1}); for the $n = 5$ member, the first cooling scan is also shown. Abbreviation: Cr_m, crystalline solid states (the XRD patterns were unable to distinguish the Cr_1 from Cr_1' phases); *Ia3d*-Cub, *Ia3d* cubic phase; *Im3m*-Cub, *Im3m* cubic phase; SmC, smectic C phase; I, isotropic liquid state. For the $n = 15$ member, the first heating curve is given as the magnified one because the *Im3m*-*Ia3d* transition was detected only on the first heating scan by DSC, although the XRD studies corresponding to the second heating scan showed the transition.

Small-Angle XRD Patterns. The Cub phase type was determined by XRD measurements. Examples of the circular-averaged XRD patterns are shown in Figure 2 and the patterns for the Cub phases of other members are compiled in the Supporting Information (see Figures S1−S3 and S5). The BABH-*n* system has two types of Cub phases; the member with $n = 13$, 15, and 16 exhibit both types. One is the *Ia3d* type. The XRD pattern was characterized by two intense and several much weaker peaks, with the absence of

(41) Ueki, T.; Hiragi, Y.; Kataoka, M.; Inoko, Y.; Amemiya, Y.; Izumi, Y.; Tagawa, H.; Muroga, Y *Biophys. Chem.* **1985**, *23*, 115–124.

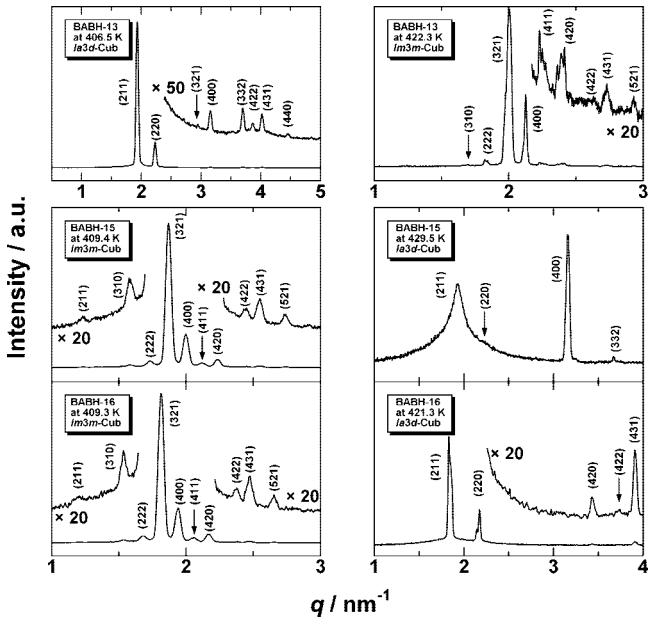

Figure 2. XRD patterns of BABH-13 (top), BABH-15 (middle), and BABH-16 (bottom) in the *Ia*3*d*-Cub and *Im*3*m*-Cub phases on heating.

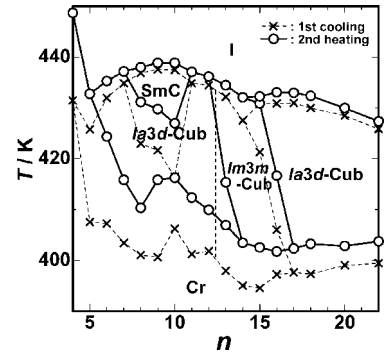

Figure 3. Phase diagram of BABH-*n*. Transition temperatures were determined by DSC both on first cooling (x and broken lines) and on second heating (open circles and solid lines). Phase type determined by POM and XRD are also shown. Abbreviation: Cr, crystalline solid state; *Ia*3*d*-Cub, *Ia*3*d* cubic phase; *Im*3*m*-Cub, *Im*3*m* cubic phase; SmC, smectic C phase; I, isotropic liquid state.

diffractions with lower indices (100), (110), (111), (200), and (210). The close inspection of the systematic absence matches the following rule: (*hkl*) with $h + k + l = 2n$, (0*kl*) with $k = 2n$ and $l = 2n$, (*hhl*) with $2h + l = 4n$, and (00*l*) with $l = 4n$ are observable, where n = integer and h, k, and l are permutable.[42,43] This rule unequivocally selected the space group *Ia*3*d* since the system is achiral. For the *Ia*3*d* phase of the $n = 15$ member, however, the (211) reflection that is usually intensely observed is very broad, and the pattern is largely deformed from that obtained for a sample with no preferred orientation. This reflects the easy growth of a small number of large Cub domains, especially at temperatures close to the isotropic liquid (I) phase. Figure S3b in the Supporting Information is a single domain pattern (two-dimensional image) obtained for the same sample at a slightly higher temperature.

Another type is the *Im*3*m* phase. In the XRD pattern, much larger number of peaks was detected as compared with the *Ia*3*d* phase mentioned above. The only rule observed for peaks detected was (*hkl*) with $h + k + l = 2n$ (n = integer), which only suggests a body-centered cubic symmetry.[42,43] Although more thorough examination is necessary, we chose the most symmetric case *Im*3*m*, as usually assumed for such body-centered Cub phases. In the case of two thermotropic systems (a binary mixture of ANBC-18 with 3,5-didodecyloxybenzoic acid and a "hemiforked" mesogen),[29] the space group was exactly confirmed to be *Im*3*m*. The intensity variation with q observed for the present system, including a feature of having the (321) peak as the most intensified one, is very similar to those observed for the above ANBC-18 system[29] and other thermotropic *Im*3*m*-Cub phases.[14,27] This suggests that the selection of the space group *Im*3*m* is appropriate and the same type of molecular aggregation structure is formed in the *Im*3*m* phase.

Phase Diagram of BABH-*n* System. The phase transition behavior of the BABH-*n* system is summarized in the phase diagram shown in Figure 3. Here, all crystalline states are simply designated Cr for clarity. The diagram was preliminarily reported in our previous publications[40] but revised carefully and finally established in the present paper. In the phase diagram, the *Im*3*m*-Cub region is in-between two *Ia*3*d*-Cub regions. The same type of phase diagram was reported for the ANBC-*n* system.[5,27d]

Cub-to-Cub Phase Transitions of the $n = 13$, 15, and 16 Members. The most important revision in the phase diagram is the presence of thermally induced Cub-to-Cub phase transition for the $n = 13$, 15, and 16 members. The XRD patterns of the two Cub phases for these three members on heating were already presented in Figure 2. In Figure S4 of the Supporting Information, the *d*-spacings of the XRD peaks are plotted vs temperature to illustrate their transformation processes. In those thermal cycles, temperature was increased/decreased at a rate of 1 K min^{-1} to each objective temperature and the temperature was kept for at least 10 min prior to the XRD measurement. As seen from Figure 2 (top) and the Supporting Information, Figure S4a, the $n = 13$ member exhibits an *Ia*3*d*-to-*Im*3*m* transition at around 412 K on heating. This XRD result is consistent with the DSC data, which detected a faint endothermic peak at 415 K on heating (Figure 1). On cooling, the high-temperature *Im*3*m* phase was about 15 K supercooled and directly transformed to the crystalline state at around 401 K (and at 397 K on DSC; not shown in Figure 1). On the other hand, the $n = 15$ member (Figure 2 (middle) and the Supporting Information, Figure S4b) exhibits on heating an *Im*3*m*-to-*Ia*3*d* transition at around 427 K on XRD (and at 430 K on first-heating DSC; see the caption of Figure 1). On cooling, the reverse transition, the *Ia*3*d*-to-*Im*3*m* transition was observed at around 421 K on XRD, but no anomaly was detected on

(42) International Union for Crystallography. *International Tables for Crystallography*, 2nd revised ed.; Hahn, T., Ed.; Kluwer Academic: Dordrecht, The Netherlands, 1989; Vol. A.

(43) In the systems with cubic symmetry, the ratios of reciprocal d of observed peaks are $\sqrt{n_1}:\sqrt{n_2}:\sqrt{n_3}$:, and the numbers ($n_1$, n_2, and n_3) inside $\sqrt{}$, or those times integer, should correspond to $h^2 + k^2 + l^2$ when the diffraction is assigned to (*hkl*) planes. Because the (*hkl*) planes with $h^2 + k^2 + l^2 = 7$ and 15 are not possible with any cubic systems, the sequence of numbers must be doubled. Indexation of diffractions assigned to (321) and (521) was made in this way (see Figures 2 and 4, and the Supporting Information, Figures S1, S2, and S4−S6).

DSC. For the $n = 16$ member (Figure 2 (bottom) and the Supporting Information, Figure S4c), on heating, an *Im*3*m*-to-*Ia*3*d* transition was observed at around 417 K on XRD and at 416 K on DSC. The behavior on cooling was slightly complicated. The high-temperature *Ia*3*d* phase was supercooled down to around 405 K, and crystallization was observed at 400 K, after the coexistence of both types of Cub phase was observed at 403 K. The corresponding DSC thermogram detected no anomaly around that temperature. However, when the sample was stored at 406 K for a prolonged time (100 min), the initially observed *Ia*3*d* phase was found to be replaced by the *Im*3*m* phase (see the Supporting Information, Figure S5). Thus, in case of the $n = 16$ member, the transition between the high-temperature *Ia*3*d* and low-temperature *Im*3*m* phases is reversible with temperature, similarly to the $n = 15$ member, but followed by a slightly larger thermal hysteresis (of about 10 K).

Examples for single compounds exhibiting phase transitions between two different Cub phases are still very rare to date[19d,27,44] and as for the transition between the *Ia*3*d*-gyroid and *Im*3*m* phases, the BABH-*n* system is the second example.

***Ia*3*d*-Cub to SmC Phase Transitions of the $n = 8-10$ Members.** The $n = 8-10$ members exhibit the SmC phase in addition to the *Ia*3*d*-Cub phase on both heating and cooling, and their transformation processes are summarized in Figure 4 (other figures of *d*-spacings vs temperature plots for BABH-*n* with $n = 5-7$, 11, 12, 14, 17, 18, 20, and 22 are compiled in the Supporting Information, Figure S6).[45] For the three members, the (211) spacing of the *Ia*3*d*-Cub phase ($d(211)$) is considerably close to the layer spacing of the high-temperature SmC phase ($d(001) = L_{SmC}$) at the transition temperature. This is an epitaxial relationship of particular planes between the lamellar and *Ia*3*d*-Cub phases, which is established in the lyotropic LC systems.[46] The observation of the same relationship in the thermotropic LC systems such as BABH-*n* is usually accepted as an analogy between both LC systems. We rather notice, however, a small difference observed between the L_{SmC} and $d(211)$. The value of L_{SmC} for $n = 8$, 9, and 10 is 1.9, 3.2, and 3.2% larger than that of $d(211)$, respectively. The same trend was seen for ANBC-*n* system and the difference between the L_{SmC} and $d(211)$ was 0.07−2.5% for $n = 15-18$,[27d] where, contrary to the BABH-*n* system, the SmC phase is at the low-temperature side of the *Ia*3*d*-Cub phase. It is thus probable that a slight expansion of the SmC layer spacing in comparison with the *Ia*3*d*-Cub (211) spacing at the phase boundary is a general trend in the thermotropic LC systems. As will be discussed later in detail, this trend is related to the lateral thermal expansion and longitudinal contraction of the alkyl chain part and/or the change in the tilt angle of the constituent molecule within the filamentary layer in the Cub phase, as compared to the state in the SmC phase.

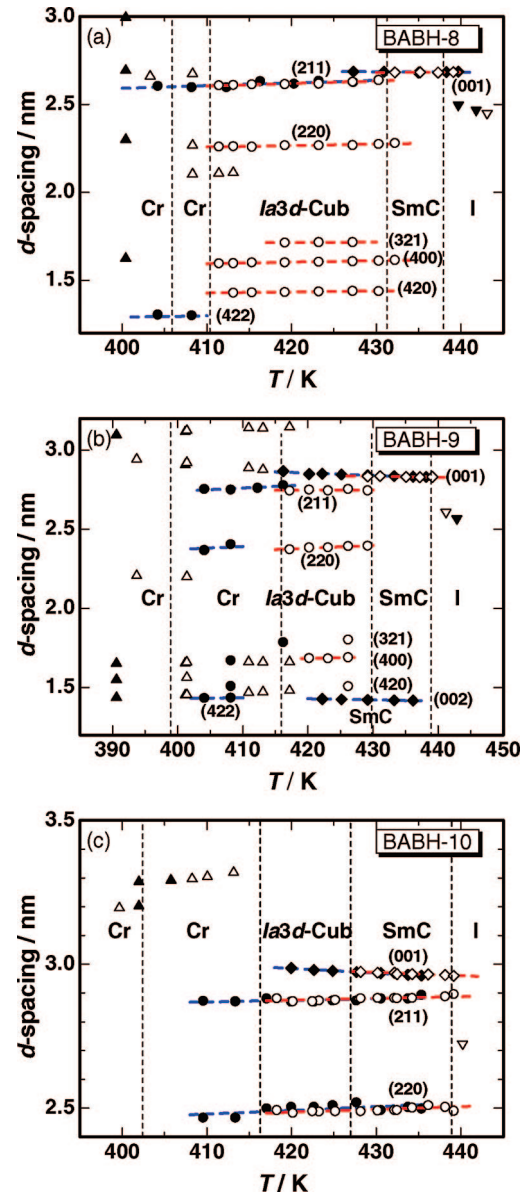

Figure 4. Variation of *d*-spacings of the XRD peaks as a function of temperature (*T*) for (a) BABH-8, (b) BABH-9, and (c) BABH-10. Both heating (open symbols, red broken lines) and cooling (closed symbols, blue broken lines) data are shown; vertical broken lines indicate phase transition temperatures determined by the second heating DSC scans.

Another issue noted in Figure 4 is the remaining of the *Ia*3*d*-Cub phase in the temperature region designated as "SmC" for the $n = 10$ member. The fraction of the Cub phase derived from the integrated intensities of both *Ia*3*d*-Cub (211) and SmC (001) diffractions changed from 0.22 to 0.12 and to 0.02 with increasing temperature from 433.4 to 436.0 K and to 438.5 K, and from 0.09 to 0.11 and to 0.19 with decreasing temperature from 433.8 to 427.7 K and to 422.7 K. Because a similar coexistence was not observed for the $n = 8$ and 9 members, we can reasonably assign the

(44) Percec, V.; Holerca, M. N.; Uchida, S.; Cho, W.-D.; Ungar, G.; Lee, Y.; Yeardley, D. J. P. *Chem.—Eur. J.* **2002**, *8*, 1106–1117, but this case is a transition between two micellar type Cub phases.

(45) For all BABH-*n*, a broad halo was detected in the small-angle region at temperatures even in the isotropic liquid I phase in the vicinity of the Cub/SmC phase, and the spacing is plotted with symbols ∇ or ▼. The selected patterns are displayed in the Supporting Information, Figure S7. The presence of such a halo indicates that there still remain the constituent aggregates that construct the Cub/SmC phase structure, which would gradually collapse in the higher-temperature region. A similar observation was reported for other Cub-phase-forming materials (see refs 15e,f, 25, 27c,d, and 56b), which also exhibit the so-called DSC "hump" both on heating and on cooling; in BABH-*n*, however, the transition peak into the I phase was followed by not a clear hump but only a tail extended at the higher temperature side (see Figure 1).

(46) Rançon, Y.; Charvolin, J. *J. Phys. Chem.* **1988**, *92*, 2646–2651.

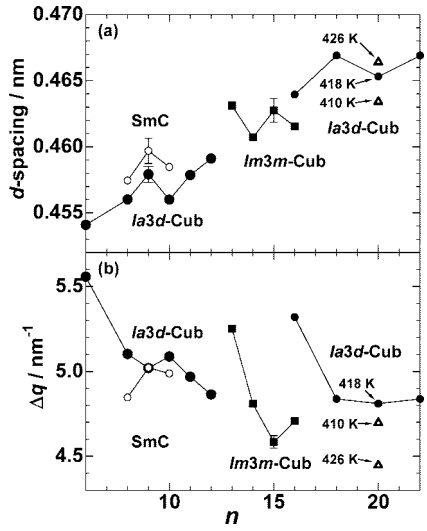

Figure 5. Variation of (a) *d*-spacing ($= 2\pi/q_{max}$) derived from the wide-angle scattering peak and (b) its full width at half-maximum (Δq) vs alkyl chain length *n* for several BABH-*n* members in the Cub and SmC phases. For $n = 9$, 15, and 20, the error bars are given from the duplicative measurements (in (b), the error bar is comparable to the symbol size); for $n = 20$, the data points for different temperatures are also shown for illustrating the temperature effect.

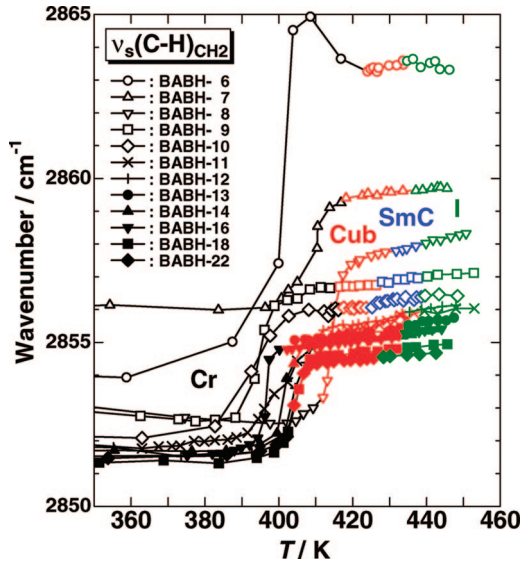

Figure 6. Temperature variation of peak frequencies of the methylene C−H symmetric stretching vibration ($\nu_s(C-H)_{CH_2}$) for several BABH-*n* members. Black, red, blue, and green symbols indicate data points for Cr, Cub, SmC, and I phases, respectively.

observation to the proximity of the free energies of both the *Ia3d*-Cub and SmC phases occurring around $n = 10$, with the order reversed for $n \geq 11$.

Wide-Angle XRD in the Mesophases. XRD patterns in the wide-angle region were also measured for several BABH-*n* members in the Cub and SmC phases. For all cases, a single broad scattering maximum attributable to the disordered state of the alkyl chains was observed at around $q_{max} = 14$ nm^{-1}, regardless of the phase type. The scattering was well reproduced by a Lorentzian function and a representative example is displayed in Figure S8 in the Supporting Information. Figure 5 summarizes the dependence of the two adjustable parameters, (a) *d*-spacing ($= 2\pi/q_{max}$) and (b) a full width at half-maximum (Δq), on alkyl chain length *n*.

Figure 5a shows that the lateral spacing of the alkyl chains in the Cub phase increases with *n*. The increase, however, becomes gentle for $n = 13-16$ that is the *Im3m*-Cub phase region (measured temperature *T* ranges from 409 to 423 K in this case) and for $n = 16-22$ that is the longer chain *Ia3d*-Cub phase region ($T \approx 420$ K); rather, the value seems constant with *n* in those phase regions. On the other hand, for $n = 8-10$, the value of the SmC phase ($T \approx 435$ K) is 0.3−0.5% larger than that of the *Ia3d*-Cub phase ($T \approx 420$ K). That change, however, seems largely due to the temperature effect if we consider the temperature change such as observed for $n = 20$. As for the behavior of Δq in Figure 5b, a relatively large value was observed for $n = 6$, 13, and 16, which are the smallest values of the three Cub phase regions (shorter chain *Ia3d*, *Im3m*, and longer chain *Ia3d* phases, respectively). This suggests that those self-organized structures contain the largest inhomogeneity among the three Cub phase regions.

Infrared in the Mesophases. To get information about the molecular level aggregation state, FT-IR spectroscopy is useful and the temperature variation measurements were carried out. One example of the temperature-dependent spectra is presented in Figures S9 and S10 in the Supporting Information.

It is well-known that the frequency of the methylene C−H symmetric stretching vibration ($\nu_s(C-H)_{CH_2}$) is sensitively influenced by an introduction of gauche conformers on the alkyl chains and shifts to higher frequencies when the gauche bond density is increased.[47] We monitored the $\nu_s(C-H)_{CH_2}$ vibration frequencies of BABH-*n* on heating, and the results are compiled in Figure 6. In all BABH-*n* examined, a sharp rise is seen before or on entering into the Cub phase (red region), thus clearly indicating that the conformational structure of the alkyl chains is fully liquidlike in the Cub phase, almost identical with that in the normal liquid I phase (green region). In other words, almost complete melting of the alkyl chains is essential for the formation of the Cub phase.[33] For $n = 8-10$, the SmC phase (blue region) appears at the high-temperature side of the Cub phase, but no noticeable change in frequency was observed in that temperature range.

Information about the hydrogen-bonding state was obtained from the N−H stretching (ν_{N-H}) vibration.[48] In the crystalline states of all members examined, the vibration was observed as a broad absorption centered at 3220−3250 cm^{-1}, reflecting the presence of a strong hydrogen bonding network (see the Supporting Information, Figure S10). The peak frequency was dependent on temperature, and the results are summarized in Figure S11 of the Supporting Information: A sharp rise was seen before or on entering into the Cub phase and the peak frequency lied in the range 3290−3300

(47) (a) Asher, I. M.; Levin, I. W. *Biochim. Biophys. Acta* **1977**, *468*, 63–72. (b) Umemura, J.; Cameron, D. G.; Mantsch, H. H. *Biochim. Biophys. Acta* **1980**, *602*, 32–44. (c) Lee, W. K.; Heiney, P. A.; Ohba, M.; Haseltine, J. N.; Smith, A. B., III *Liq. Cryst.* **1990**, *8*, 839–850.
(48) (a) Nakamoto, K.; Margoshes, M.; Rundle, R. E. *J. Am. Chem. Soc.* **1955**, *77*, 6480–6486. (b) Wang, F. C.; Feve, M.; Lam, T. M.; Pascault, J.-P. *J. Polym. Sci., Part B: Polym. Phys.* **1994**, *32*, 1305–1313.

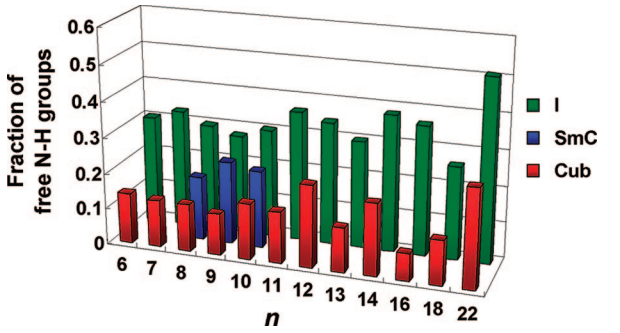

Figure 7. Fraction of free N−H groups in three phases (Cub, SmC, and I phase) as a function of *n* for BABH-*n*. For the three phases, temperatures selected are 423 ± 1.5, 434 ± 1, and 443 ± 1 K, respectively.

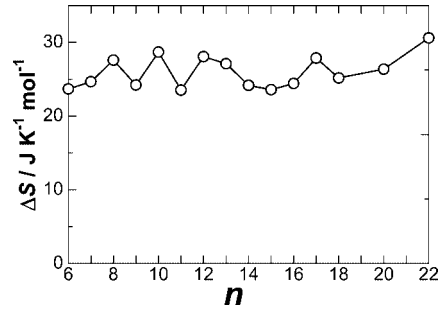

Figure 8. Sums of the entropies (Δ*S*) obtained above the melting point until isotropization as a function of *n* for BABH-*n*.

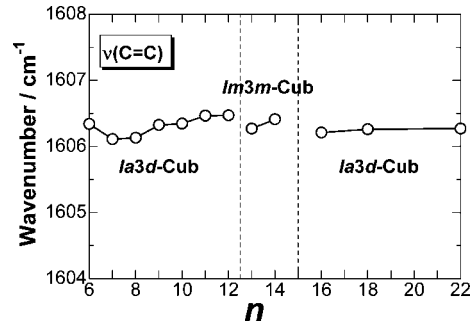

Figure 9. Variation of peak frequencies of the aromatic C═C stretching vibration (ν(C═C)) versus alkyl chain length *n* for several BABH-*n* members in the Cub phase. Temperatures selected are 424 ± 1 K.

cm^{-1} in the Cub and SmC phase region. Qualitatively, this temperature dependence can be attributed to weakening of the intermolecular hydrogen bonding, which is necessary for the constituent molecules obtaining mobility within those phases. Probably, the hydrogen bonding would have more dynamic nature, unlike in the crystalline state, changing its counterpart from time to time.

In that temperature region, the band profile was composed of at least two components, one at 3390−3400 cm^{-1} which is associated with free N−H groups and the other at 3270−3310 cm^{-1} coming from weakly hydrogen-bonded N−H ones. In order to estimate the influence of the latter intermolecular hydrogen bonding on the formation of the Cub and SmC phases, we resolved the band profile into the two components (a typical example is illustrated in Figure S12 of the Supporting Information[49]) and then, the fraction of free N−H groups was evaluated. In this evaluation, the ratios of molar absorption coefficients corresponding to two different states of N−H groups were calculated for each *n* and used (see the Supporting Information, Figure S13 and Table S2).[48b,50] The fractions of free N−H groups as a function of temperature for all BABH-*n* examined are compiled in the Supporting Information, Figure S14, and the representative values determined in this way for three phases (Cub, SmC, and I phases) are plotted as a function of alkyl chain length (*n*) in Figure 7. In the Cub phase (the selected temperatures are 423 ± 1.5 K), the fraction lies in the range 0.11−0.15, almost independent of *n* for $6 \le n \le 12$, where the Cub phase type formed is *Ia*3*d*. The fractions for $n =$ 13 and 14 that exhibit an *Im*3*m* type are 0.12 and 0.20, respectively. A further increase in *n* again produces an *Ia*3*d* type, where the fraction varies from 0.08 for $n = 16$ to 0.28 for $n = 22$, dependent on *n*. This result strongly suggests that there is some difference in the lateral core−core interaction between the two *Ia*3*d* groups formed by shorter and longer alkyl chain members. This will be discussed later in more detail.

For $n = 8-10$, the fraction in the SmC phase (the selected temperatures are 434 ± 1 K) is 0.18−0.23, 35−100% larger than that in the respective Cub phase; the lateral core−core interaction in the SmC phase is weaker than in the Cub phase. In the normal liquid I phase (443 ± 1 K), the fraction reaches 0.3−0.5 and thus about half of the molecules are isolated in this state. This demonstrates that in the Cub phase, the intermolecular hydrogen bonding, which is of course weaker than in the crystalline states, is essential for the formation and stabilization of that phase.

To summarize the interplay between the hydrogen bonding and alkyl chains, it may be roughly said that thermally activated alkyl chain is a trigger to the formation of the Cub phase while the lateral core−core aggregation is maintained to some extent through the intermolecular hydrogen bonding at those temperatures, but at higher temperatures, the hydrogen bonding no longer able to bundle the cores, which leads to the destruction of the Cub phase structure. The last comment is also supported by the following thermodynamic analysis: as shown in Figure 8, the entropic gain per molecule above the melting temperature (Δ*S*) is almost independent of the alkyl chain length *n*.

Finally, we examined the aromatic C═C stretching (ν(C═C)) band in the Cub phase temperature region. Figure 9 plots the peak frequency against *n*, where the frequency was determined by fitting the peak top with a cubic polynomial. The frequency seems almost around 1606.2 cm^{-1}, but a closer look indicates a difference between the shorter and longer chain *Ia*3*d* phase regions: a faint increase from 1606.1 cm^{-1} for $n = 8$ to 1606.5 cm^{-1} for $n = 12$ whereas a constant value of 1606.2 cm^{-1} from $n = 16$ to

(49) Absorption in the range 3030−3150 cm^{-1}, which has two evident peaks at 3040 and 3070 cm^{-1}, is assigned to the C−H stretching vibrations of the benzene ring, and a shoulder peak around 3200 cm^{-1} is probably the two-phonon band of the C═O fundamental vibration observed at around 1640 cm^{-1}.[48b] Thus, the curve-fitting procedure was performed in the range 3250−3600 cm^{-1}.

(50) The determined ratios of molar absorption coefficients ($\epsilon_{\text{H-bonded N−H}}/\epsilon_{\text{free N−H}}$ with $\epsilon_{\text{H-bonded N−H}}$ and $\epsilon_{\text{free N−H}}$ being the coefficients for hydrogen-bonded and free N−H vibration bands, respectively) depended on *n* and ranged between 5.1 and 9.7 (see the Supporting Information, Table S2). More detailed procedures are described in the Supporting Information, Figure S13.

22. The higher frequency shift in the shorter chain *Ia*3*d* phase regions may be related to weakening of the intermolecular $\pi-\pi$ interaction of BABH-*n* molecules, because if conjugation between the neighboring aromatic rings occurs, it weakens the force constant of the aromatic C=C bonds and causes a lower frequency shift. Although the shift certainly seems obscure, it was actually reproducible and at least gives us a hint for our question what are different between the two *Ia*3*d* phases, which will be discussed later.

Discussion

Features of the Cub Phase Formation in the BABH-*n* System. The phase diagram of the BABH-*n* system (Figure 3) contains several features:

First, the Cub phase formation is seen in a very broad range of $n = 5$ - 22 (at present) and more. The broad range of n also changes the weight fraction of the alkyl chain largely, from 0.34 for $n = 5$ to 0.70 for $n = 22$, almost twice. This observation is in contrast with the lyotropic systems, where the formation is usually limited in a narrow concentration region sandwiched between the lamellar and hexagonal columnar phases.[51]

Second, the Cub region contains the formation of two types of Cub phases, and the phase sequence of *Ia*3*d*−*Im*3*m*−*Ia*3*d* along with lengthening the chain is a general trend for the Cub-phase-forming molecules, at least, with the following molecular features: a central slightly polar aromatic core with one flexible chain attached to each end (such as seen in the ANBC-*n* and BABH-*n*).

Third, when seen along with temperature variations at a constant n, the members with $n = 13$, 15, and 16 exhibit a Cub-to-Cub phase transition. Among one-component thermotropic systems, a Cub-to-Cub phase transition was first found for the ANBC-*n* series with $n = 22$ and 26; the *Im*3*m* phase was transformed into the *Ia*3*d* phase on heating but no reverse transition was observed in that system.[27] For the BABH-*n* series, the transition between the *Im*3*m* and *Ia*3*d* phases observed for $n = 15$ and 16 is similar to those seen in the ANBC-*n* series in that the *Ia*3*d* phase is located at the higher temperature side, whereas it is different in that the transition is observed as being reversible with temperature. Moreover, for $n = 13$, the situation that the *Ia*3*d* phase is located at the lower temperature side is realized, although the transition was seen in this case only on heating. The third feature was found for the first time for the present system.

Different phase sequences regarding the Cub phases on increasing temperature between the $n = 13$ member and the $n = 15$ and 16 members seem quite unusual, but can be well-explained in terms of the quasibinary picture model:[26] The previous entropy analysis on the *Ia*3*d* and *Im*3*m* phases for the ANBC-*n* series revealed that the alkyl chain is more disordered in the former phase than in the latter and when lengthening the chain, the difference increases by 0.18 J K^{-1} (mol of CH_2)$^{-1}$ in terms of entropy.[32c] Assuming that the same situation holds for the BABH-*n* series and the absolute entropy of the core arrangement (and accompanied dynamics) remains the same for each of these phases, the entropy of the transition between them directly reflect the difference in the chain entropy. In that case, the reversal in sign of the entropy of the transition is readily expected upon the elongation of the chain as illustrated in Figure 10, where n_C is the number of alkyl carbon atoms within a molecule. Since the entropy is always positive in any temperature-induced first-order phase transitions, the change in sign results in the inversion of the phase sequence. Here, one question arises whether the slope is the same as in the ANBC-*n* series. The slope determined preliminarily by the present DSC measurements was ∼+0.3 J K^{-1} (mol of CH_2)$^{-1}$.

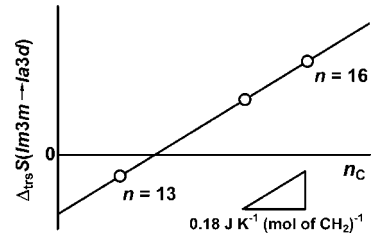

Figure 10. Schematic illustration expected for the entropy of the transition from *Im*3*m*- to *Ia*3*d*-Cub phases upon the elongation of the chain. The slope 0.18 J K^{-1} (mol of CH_2)$^{-1}$ was obtained for a similar Cub-phase-forming system ANBC-22.[32c]

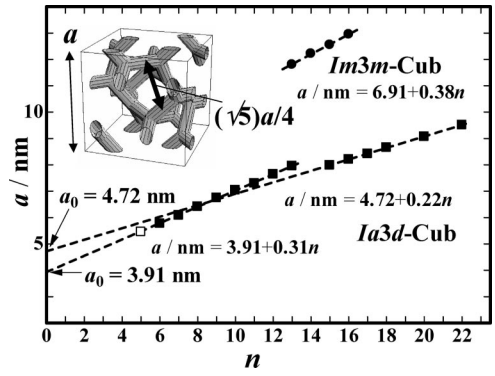

Figure 11. Plots of the Cub lattice parameter a vs alkyl chain length n, where three broken lines represent least-squares fits for the data; the data for $n = 5$ is omitted for the fitting because it was obtained from the cooling process. The selected temperatures are compiled in Table 1. The 3-by-3 network model for the *Ia*3*d*-Cub phase is also illustrated.

Lattice Parameter *a* vs Alkyl Chain Length *n*. Figure 11 plots the lattice parameter a vs alkyl chain length n for the two Cub phases. There are three regions where linearity of a vs n is valid. The straight lines were determined by using least-squares fits for the data: a/nm = 3.91 + 0.31n for the *Ia*3*d* phase of $6 \le n \le 13$, a/nm = 6.91 + 0.38n for the *Im*3*m* phase of $13 \le n \le 16$, and a/nm = 4.72 + 0.22n for the *Ia*3*d* phase of $15 \le n \le 22$. The increment of the a with respect to n for the *Im*3*m* phase is 1.7 times larger than that for the *Ia*3*d* phase in the longer chain BABH-*n* members. If one simply regard that the Cub phase structure is composed of deformed smectic layers, interfaces between the two neighboring layers correspond to the so-called triply periodic minimal surfaces (TPMSs). When n is increased by one, the thickness of the single layer is increased by the length of two methylene units. Thus, the almost doubled increment observed can be assigned to

(51) Fairhurst, C. E.; Fuller, S.; Gray, J.; Holms, M. C.; Tiddy, G. J. T. In *Handbook of Liquid Crystal*; Demus, D., Goodby, J., Gray, G. W., Spiess, H.-W., Vill, V., Eds.; Wiley-VCH: Weinheim, Germany, 1998; Vol. 3, pp 341−392.

Table 1. Parameters of the Cub and SmC Phases in BABH-*n*[a]

n	T_{Cub} (K)	space group	*a* (nm)	a^3 (nm^3)	*N*	S_{Cub} (nm^2)	N_{rod}	N_{slice}	l_{core} (nm)	V_{alkyl} (nm^3)	V_{core} (nm^3)	V_{alkyl} + V_{core} (nm^3)	d_{core} (g cm^{-3})	V_{alkyl}/a^3	T_{SmC} (K)	L_{SmC} (nm)	S_{SmC} (nm^2)
						G-TPMS				Bundle Type							
5	419.7	*Ia3d*	5.46	163	237	0.388	9.9	2.31	2.19	42	121		1.15	0.26			
6	423.3	*Ia3d*	5.77	192	263	0.392	11.0	2.42	2.19	61	132		1.18	0.32			
7	423.9	*Ia3d*	6.09	225	290	0.395	12.1	2.52	2.19	83	142		1.20	0.37			
8	423.3	*Ia3d*	6.42	264	320	0.397	13.3	2.65	2.19	110	154		1.22	0.42	435.2	2.68	0.308
9	423.6	*Ia3d*	6.75	307	352	0.399	14.7	2.77	2.19	141	166		1.25	0.46	435.1	2.83	0.308
10	423.3	*Ia3d*	7.04	349	380	0.403	15.8	2.86	2.19	173	176		1.27	0.50	434.1	2.98	0.309
11	422.6	*Ia3d*	7.30	389	403	0.408	16.8	2.93	2.19	206	183		1.30	0.53			
12	423.3	*Ia3d*	7.64	446	441	0.409	18.4	3.06	2.19	250	196		1.33	0.56			
13	407.3	*Ia3d*	7.95	503	476	0.411	19.8	3.17	2.19	296	207		1.35	0.59			
										Rod Type							
15	429.5	*Ia3d*	7.98	509	442	0.446	18.4	2.94	2.64	276	237	513	1.27	0.54			
16	423.3	*Ia3d*	8.21	553	462	0.451	19.2	2.98	2.64	314	248	562	1.27	0.57			
17	423.3	*Ia3d*	8.42	597	480	0.457	20.0	3.02	2.64	352	258	610	1.27	0.59			
18	421.3	*Ia3d*	8.65	648	502	0.461	20.9	3.08	2.64	397	268	665	1.27	0.61			
20	423.2	*Ia3d*	9.07	746	539	0.472	22.5	3.15	2.64	487	288	775	1.28	0.65			
22	421.2	*Ia3d*	9.51	861	583	0.480	24.3	3.25	2.64	591	308	899	1.29	0.69			
						PP-TPMS											
13	416.2	*Im3m*	11.80	1644	1555	0.367		2.45									
14	415.4	*Im3m*	12.22	1824	1652	0.371		2.51									
15	415.3	*Im3m*	12.55	1978	1719	0.376		2.54									
16	415.3	*Im3m*	12.95	2172	1814	0.379		2.60									

[a] Keys: *n*, number of carbon atoms in the alkyl chain; T_{Cub}, Cub phase temperature; *a*, Cub lattice parameter; a^3, Cub lattice volume; *N*, number of molecules per Cub unit lattice, which is calculated assuming the bulk density is 1 g cm^{-3}; S_{Cub}, interface area per molecule of the Cub phase,which is calculated using the relation $S_{Cub} = 3.091a^2/N$ for G-TPMS[52] and $S_{Cub} = 4.097a^2/N$ for PP-TPMS;[52] N_{rod}, number of molecules contained in one rodlike micelle for the *Ia3d* phase, which is calculated using the relation $N_{rod} = N/24$; N_{slice}, number of molecules per 0.45 nm thick slice of rod and for the *Im3m* phase, calculated assuming that the total length of rods per unit lattice is given by $24.216a$;[29] l_{core}, effective core length determined by the *a* vs *n* plot (see Figure 11); V_{alkyl}, liquidlike alkyl chain volume calculated using the following values by Reiss-Husson and Luzzati (CH_3, 0.0595 nm^3; CH_2, 0.028 nm^3);[19f,53] V_{core}, effective core volume, which is calculated assuming a 3-by-3 network of rods with a diameter of l_{core} for the longer alkyl chain *Ia3d* phase, and for the shorter chain *Ia3d* phase, obtained by subtracting V_{alkyl} from a^3; d_{core}, local density within the effective core region; T_{SmC}, SmC phase temperature; L_{SmC}, SmC layer thickness; S_{SmC}, interface area per molecule of the SmC phase, which is calculated using the relation $S_{SmC}/\text{nm}^2 = M/[(10^{-21}\ \text{g nm}^{-3})N_A L_{SmC}]$ with *M* being the molecular mass (in g mol^{-1}) and N_A Avogadro's number (in mol^{-1}) and assuming the bulk density is 1 g cm^{-3}.

the presence of twice the number of TPMSs, for example, along the face diagonal line per unit lattice, in the *Im3m* phase compared to the *Ia3d* phase. This supports a PP-TPMS structure as the first-order approximation, as in the case of the ANBC-*n* series.[5,26d,28] One might, however, point out that the difference is only 1.2 times when using the increment for the *Ia3d* phase in the shorter chain members, which might contradict the validity of the PP-TPMS structure. However, we should take it into consideration that in the shorter chain members the alkyl chain length is not enough to regard all the methylene units equally behave in the Cub phase (This will be discussed in the next section). Another fact to consider is the contribution of the hydrogen bonding acting laterally between neighboring molecules. The above logic for the PP-TPMS structure is valid as long as the alkyl chain is a major contribution to d*a*/d*n*. Therefore, the 1.2 times difference does not rule out the validity of the PP-TPMS structure for the *Im3m* phase.

Packing Study for Two *Ia3d*-Cub Phases. Table 1 compiles characteristic parameters of the Cub and SmC phases of BABH-*n* with various chain length *n*. In this table, all calculations were made with an assumption that the density is 1 g cm^{-3}.

As mentioned in the Introduction, the *Ia3d*-Cub structure has two important positions, G-TPMS and 2-fold axes, and the latter parts are linked with each other to form two pairs of 3-by-3 interpenetrating networks. For the present system, the distance between the two neighboring G-TPMSs corresponds to a molecular length, and so, if the methyl end groups of the alkyl chains are located on the surfaces, the aromatic cores are on the 3-by-3 networks and vice versa. In the previous X-ray diffraction analyses,[40b] we revealed that the former case is valid for all *Ia3d* phases of BABH-*n* with $n = 5-13$ and $15-22$; the aromatic cores aggregate to form rods which construct two pairs of 3-by-3 networks, while the remaining space is filled by the alkyl chains. The number of such rods within a unit lattice is 24, and so the number of molecules in a rod (N_{rod}) is given by $N_{rod} = N/24$, with *N* being the total number of molecules in a unit lattice. Since the length of each rod is $a/\sqrt{8}$, with a lattice parameter of *a*, we can obtain the number of molecules per 0.45 nm thick slice of the rod (N_{slice}) (From Figure 5, if we suppose the *d*-spacing corresponds to the lateral intermolecular periodicity, it is around 0.455−0.465 nm, but we used 0.45 nm for simplicity). The values obtained for various *n* lie in the range 2.3−3.3, which should be regarded as the lower limit because the above calculation neglects the presence of junction points where three rods join. The real values of N_{slice} would be slightly larger and we can derive a conclusion that, boldly speaking, 3−4 molecules are in the slice.

For the *Im3m* phases, if we adopt the Zeng−Ungar−Clerc model,[29] the total length of rods per unit lattice is given by

(52) Schwarz, U. S.; Gompper, G. *Phys. Rev. E* **1999**, *59*, 5528–5541.
(53) (a) Reiss-Husson, F.; Luzzati, V. *J. Phys. Chem.* **1964**, *68*, 3504–3511. (b) Their values (v_{CH_3} and v_{CH_2}) were evaluated for 70 °C, but we used without correcting the temperature effect, because of the expectation that the partial volumes are more or less reduced for the alkyl chains with one end attached to an aromatic core such as in our case.

24.216a, and the values of N_{slice} obtained for $n = 13-16$ are 2.5−2.6. In their model, the networks of rods are so complicated; there are three types of junction points where two, three, or five rods meet. Thus, it is probable that the real N_{slice} is almost the same as in the *Ia*3*d* phases.

In order to consider the state of the methyl end groups, the alternative description for the Cub phases, the TPMS picture, is useful. For the *Ia*3*d*-Cub phases, the average cross-section area per alkyl chain (S_{Cub}) is given by a relation of $S_{Cub} = 3.091a^2/N$.[52] The value of S_{Cub} obtained in this way is dependent on n, going from 0.39 for $n = 5$ to 0.48 nm^2 for $n = 22$. In case of $n = 8-10$, both *Ia*3*d* and SmC phases are formed. The values of S_{Cub} are ca.0.40 nm^2, whereas the corresponding values for the SmC phases (S_{SmC}) are ca. 0.31 nm^2, implying that the alkyl chains are more extended along the molecular axis in the SmC phase than in the *Ia*3*d* phase; the corresponding observation by XRD is that the SmC layer thickness is slightly larger than the *Ia*3*d*-(211) spacing at the phase boundary, as already mentioned. This seems to imply that the entropy of the alkyl chain part slightly decreases when the *Ia*3*d* phase transitions into the high-temperature SmC phase, which is at first sight funny. However, Saito-Sorai's quasibinary picture model[26] gives a clear explanation for this; the translational degree of freedom of the aromatic core part is increased when going from "along a rod" in the *Ia*3*d* phase to "within a layer" in the SmC phase, gaining more entropy, and thus, the total entropy of the SmC phase can be larger than the *Ia*3*d* phase. In case of the *Im*3*m* phases, if we adopt the PP-TPMS model and use a relation of $S_{Cub} = 4.097a^2/N$,[52] the value of S_{Cub} lies in the range 0.37−0.38 nm^2. At this stage, however, it is not clear whether the alkyl tails are on the PP surface.

What is different between the structures of *Ia*3*d* phases formed by shorter and longer chain members? The answer can be assessed from the different dependence of the lattice parameter a on the chain length n: a/nm $= 3.91 + 0.31n$ for $6 \le n \le 13$ and a/nm $= 4.72 + 0.22n$ for $15 \le n \le 22$ (Figure 11). We consider that the value extrapolated to $n = 0$, a_0, is related to an effective core size with alkyl chains outside being in the molten state (l_{core}). Because the distance between the two facing rods is expressed as $(\sqrt{5})a/4$ (see the inset of Figure 11),[8,27b,c] the l_{core} may be estimated by $(\sqrt{5})a_0/4$. We obtain $l_{core} = 2.19$ nm for the shorter chain members and $l_{core} = 2.64$ nm for the longer ones. On the basis of the energy-minimized molecular conformation at the semiempirical PM3 level, the molecular lengths of BABH-3 and -5 are calculated to be 2.12 and 2.62 nm, respectively, and thus, those effective cores contain three and five carbon atoms of their alkyl chains, respectively. To calculate the effective core volume in a unit cell (V_{core}), we assume that the effective cores form a cylinder-like rod attached by corns with the corn angle of 120° at both ends. The volume of the alkyl chains in the molten state (V_{alkyl}) is, on the other hand, evaluated by using the values of partial specific volumes for methyl and methylene units (v_{CH_3} and v_{CH_2}) determined experimentally by Reiss-Husson and Luzzati.[19f,53] For the *Ia*3*d* phases formed by longer chain members, the sum of the V_{core} and V_{alkyl} calculated in this way is in good agreement with the corresponding value of the unit cell volume a^3 within errors of 5%. Moreover, the densities of the core region (d_{core}) are estimated at 1.27−1.29 g cm^{-3}, which are reasonable values considering the rough estimation procedure and referring to the densities (ρ) of analogous compounds in the literature: ρ of acetanilide ($C_6H_5NHCOCH_3$) in the crystalline state is 1.219 g cm^{-3} and that of acetophenone ($C_6H_5COCH_3$) is 1.033 g cm^{-3}.[54] Thus, we can derive an important conclusion that a quasibinary picture model is semiquantitatively valid for the longer alkyl *Ia*3*d* phases; the system is composed of an effective core region of a cylinder type and the remaining space is filled by molten alkyl chains. The concept of effective core having a small amount of alkyl atoms near the core was first addressed by one of the authors in their quasibinary picture model.[26b]

For the *Ia*3*d* phases formed by shorter chain members, it is also possible to express the unit lattice volume as the sum of V_{core} and V_{alkyl} but with a larger deviation of 6−14%. In this case, a more serious problem is that the estimated values of d_{core} were 1.42−1.57 g cm^{-3}, unrealistically high. We believe that the core part is coarser. Moreover, it is easily imagined that in the shorter chain members, the chain is too short to wrap all the periphery of the core region. Thus, it is more probable that the aggregation is not a cylinder-like but a bundle-type micelle having a square section; such a type of micelles was visualized by Yoneya et al.[39b] in their molecular dynamics simulation studies for BABH-8. The volume of the bundle-type core part is estimated by subtracting the molten alkyl chain part outside the alkyl C_3 atoms from the unit lattice volume a^3, and the resulting d_{core} is 1.15−1.35 g cm^{-3}, quite realistic. The values of d_{core} for $n = 12$ and 13 are still as high as 1.33−1.35 g cm^{-3}, but it is quite reasonable to consider that such high densities cause considerable frustration on the core packing, which may be an origin for the formation of the *Im*3*m* phase instead of the *Ia*3*d* phase with larger n. The schematic illustration for micelles with a bundle type and a cylinder type is given in the Supporting Information, Figure S15.

Comparison of the two *Ia*3*d* phases formed by shorter and longer alkyl chain BABH-*n*s suggests the presence of two important mechanisms on the self-organization: (i) preferential orientation of the long axes of the aromatic core parts parallel to each other and (ii) microsegregation between the two chemically incompatible parts, the aromatic core and alkyl chain parts of the molecules. In the shorter chain members, the former mechanism favors the bundle-type micelles, where the outside molten chains act as a kind of lubricant and assist the molecular mobility but interface between the two chemically incompatible parts is not necessarily energy-minimized. On the contrary, in the longer chain members, the microsegregation forms cylinder-like micelles connected 3-by-3, where the preferential orientation is considerably weakened. It can be said that the BABH-*n* system provides a broad range of self-organization process from the low molecular mass LC regime to the microsegregation regime. Because the formation of the *Im*3*m*-Cub phases is realized at the borderline between the two regimes, this also shows us why the *Im*3*m*-Cub phase is restricted to

(54) *Merck Index*, 8th ed.; Stecher, P. G., Windholz, M., Leahy, D. S., Eds.; Merck: Rahway, NJ, 1968.

the thermotropic LC systems and not seen for the lyotropic LC and block copolymer systems.

Average Molecular Shape As a Function of *n* and *T*. In the section of IR, we mentioned that interplay between the hydrogen bonding and lateral thermal expansion of the alkyl chains is crucial for the formation and stability of the Cub phase. When considering the temperature variation of the average molecular shape, the above two factors give competitive effects. We calculated the van der Waals volumes of the BABH-*n* molecules with various chain lengths *n* by using Winmostar (developed by Norio Senda) as a software. The molecular volumes are divided into two parts and almost equality of the volume fractions of the two parts (0.237 nm^3 for the alkyl chain and 0.234 nm^3 for the core part) is realized for the $n = 7$ member (although of course assuming $T = 0$ K). If the two factors are equally balanced to give the same section area at the top and central core parts, the molecular shape can be regarded as a rod, which can be easily packed side by side to form a flat layer such as in the SmA or SmC phase. However, when the alkyl chain is thermally activated and expands laterally, the molecular shape is no longer rodlike, becoming a two-megaphone-connected shape with both ends expanded. Side-by-side packing of those molecules would cause some frustration, if keeping the flat layer. Instead, a saddle surface arrangement would be stabilized, which leads to the bicontinuous-type Cub phase formation. When temperature is further elevated, weakening or dissociation of the intermolecular hydrogen bonding would proceed to reduce the above frustration, which can be visualized as the central core part being expanded, putting back the shape into a rod. This is the case of the SmC phase formation for $n = 8-10$.[55] Thus, the competition of the Cub and SmC phase formation is understood in terms of the average molecular shape dependent on temperature.

Lattice Parameter *a* vs Temperature *T*. The Supporting Information, Figure S16, compiles the *a* vs *T* curves for all BABH-*n* examined, and Table 2 summarizes the average temperature variations $[(1/a_0)(da/dT)]$, where a_0 is the value at a mid temperature in each Cub phase region. In case of the *Ia*3*d*-Cub phase, the value of $(1/a_0)(da/dT)$ is positive for $n \leq 11$ and the absolute value becomes larger for decreasing *n* from $n = 11$, whereas the larger negative values of $(1/a_0)(da/dT)$ for increasing *n* from $n = 13$, although there are some irregularities; the $n = 12$ member is located at the boundary of this trend and shows a positive da/dT on heating and a negative one on cooling. One large exception is the case of $n = 15$, where the values on heating and on cooling show a large discrepancy. This may be partly because this member stands in the vicinity of the *Im*3*m*−*Ia*3*d* phase boundary and partly because the phase region has a small temperature interval of only 4 K on heating, with being neighbored with the isotropic liquid I phase. In case of the *Im*3*m* phase, a similar trend is seen that the value is positive for $n = 13$ on heating and after that the corresponding value becomes negative and larger for increasing *n* except $n = 15$ on cooling. In thermotropic Cub systems, the values of $(1/a_0)(da/dT)$ reported are usually negative,[19f,27a,c,d,28,56] and so the present system is a very rare case.

Table 2. Temperature Dependence of Cubic Lattice Parameter (*a*) in BABH-*n*[a]

		$(1/a_0)(da/dT)$ ($\times 10^{-4}$ K^{-1})	
n	space group	on heating	on cooling
5	*Ia*3*d*		2.6
6	*Ia*3*d*	12.0	5.1
7	*Ia*3*d*	4.4	4.0
8	*Ia*3*d*	4.3	5.7
9	*Ia*3*d*	3.8	5.1
10	*Ia*3*d*	3.5	3.6
11	*Ia*3*d*	0.4	1.0
12	*Ia*3*d*	0.6	−2.4
13	*Ia*3*d*	−5.6	
15	*Ia*3*d*	−13.4	1.0
16	*Ia*3*d*	−5.7	−2.7
17	*Ia*3*d*	−0.5	−1.1
18	*Ia*3*d*	−0.6	−2.0
20	*Ia*3*d*	−1.8	−2.8
22	*Ia*3*d*	−3.1	−4.9
13	*Im*3*m*	3.1	−1.8
14	*Im*3*m*	−0.3	−3.2
15	*Im*3*m*	−0.6	2.5
16	*Im*3*m*	−2.4	−9.9

[a] Key: a_0, lattice parameter at a mid temperature of each Cub temperature region.

Clearly, the two competitive contributions considered also influence the temperature (*T*) dependence of the Cub lattice parameters (*a*). If increasing temperature enlarges the deviation of the molecular shape from a rod, the slope da/dT is negative because at the higher temperature, the smaller number of molecules constructs a Cub lattice. Such a situation is realized for $n = 13$ or larger, where the alkyl chain contribution is predominant and the intermolecular hydrogen bonding dissociation acts as a minor role even at the high temperature side of the Cub phase. Conversely, for $n = 11$ or smaller, the effect of intermolecular hydrogen bonding dissociation overcomes the alkyl chain contribution, especially at higher temperatures, which puts back the molecular shape toward a rod. This trend implies that at the higher temperatures, the larger number of molecules is needed to form a Cub lattice, thereby a positive slope of the da/dT results. In case of BABH-*n* with $n \leq 7$, it should be expected that the alkyl chain is short and the core part is more voluminous, and thus resulting in a megaphone shape with the core part expanded. Such a shape, of course, could lead to the formation of a Cub phase above the melting temperature, but if this were true, the core part should be located on the minimal surface. As already reported,[40b] such structural inversion was not observed and the reality is that the aromatic cores are on the 3-by-3 networks and the methyl end groups are located on the G-TPMS for all *Ia*3*d* phases of BABH-*n* with $n = 5-13$ and $15-22$. Moreover, we discussed and concluded that the aggregation is a bundle-type micelle with a square section rather than a cylinder-like micelle in the shorter chain *Ia*3*d* phase region. The slope

(55) For the $n = 11$ and 12 members, a rod shape is no longer realized until isotropization; only under a slight hydrostatic pressure is the SmC phase again observed.[38b,c]

(56) (a) Donnio, B.; Heinrich, B.; Gulik-Krzywicki, T.; Delacroix, H.; Guillon, D.; Bruce, D. W. *Chem. Mater.* **1997**, *9*, 2951–2965. (b) Kutsumizu, S.; Saito, K.; Nojima, S.; Sorai, M.; Galyametdinov, Y. G.; Galyametdinova, I.; Eidenschink, R.; Haase, W. *Liq. Cryst.* **2006**, *33*, 75–84.

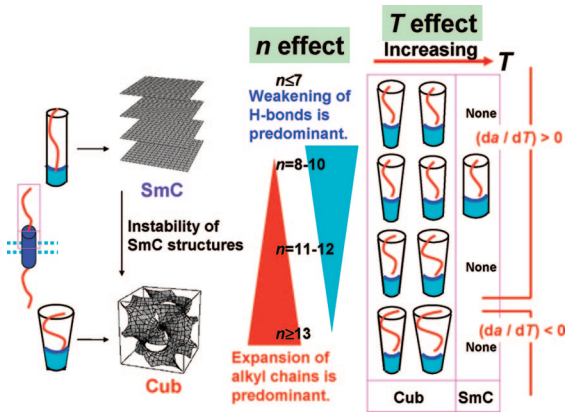

Figure 12. Schematic illustration of average molecular shape as a function of alkyl chain length n and temperature T. The molecular structure is composed of two parts, a central aromatic core part (blue region) and terminal alkyl chains (white region), and only half of the molecule is depicted for clarity. Two factors, lateral thermal expansion of the alkyl chains and thermal dissociation of intermolecular hydrogen bonding between the neighboring core parts, are considered and the former contribution becomes predominant with increasing n (n effect). When considering the temperature variation of the molecular shape (T effect), for the shorter n, the hydrogen bonding contribution is predominant at higher temperature, which leads to a positive slope of the da/dT; in the longer n ($n \geq 13$), the major contribution comes from the alkyl chain part, and then a negative slope of the da/dT results. The details are described in the text.

da/dT being positive is seen for $n \leq 7$, but the simple molecular shape consideration seems no longer valid. Figure 12 summarizes and illustrates how the molecular shape influences the self-organization of BABH-n molecules.[57]

Conclusion

In the present studies, the Cub phase formation of the BABH-n system was examined and characterized by combined techniques of DSC, POM, XRD, and FT-IR. The phase diagram of BABH-n was fully established as functions of alkyl chain length n and temperature. In the diagram, the Cub phase formation is induced in a range of $n = 5-22$, which is previously unencounteredly broad, where two bicontinuous type Cub phases with *Ia*3*d* ($n = 5-13$, $15-22$) and *Im*3*m* ($n = 13-16$) symmetries are included; at a given temperature is seen the phase sequence of *Ia*3*d*−*Im*3*m*−*Ia*3*d* with increasing n. One of the important findings is that the members with $n = 13$, 15, and 16 exhibit a Cub-to-Cub phase transition when temperature is varied; the low-temperature phase is an *Ia*3*d* phase for $n = 13$, whereas an *Im*3*m* phase for $n = 15$ and 16. As for the transition between the *Ia*3*d* and *Im*3*m* phases, the BABH-n system is the second example. This finding is significant for access to a more detailed analysis of the transformation between the *Ia*3*d* and *Im*3*m* phases and the molecular packing structure of the latter *Im*3*m* phase. The investigation along these lines is in progress in our laboratories.

The temperature variation of the Cub lattice parameter can be closely connected with a change in the average molecular shape depending on the alkyl chain length n and temperature. The interplay between the hydrogen bonding and alkyl chains is an origin for the temperature-responsive shape change; thermally activated alkyl chain is a trigger to the formation of the Cub phase while the lateral core−core aggregation is maintained to some extent through the intermolecular hydrogen bonding at those temperatures, but at higher temperatures, the hydrogen bonding no longer able to bundle the cores, which leads to the destruction of the Cub phase structure.

Finally, from the packing study for the two *Ia*3*d*-Cub phases formed by shorter and longer chain members, we have revealed that (i) preferential orientation of the long axes of the aromatic core parts parallel to each other and (ii) microsegregation between the aromatic core and alkyl chain parts of the molecules are two important competitive mechanisms on the self-organization. In the shorter chain members, the former mechanism is effective to form bundle-type micelles which lie on the 3-by-3 network lines, whereas the microsegregation preferentially contributes to form cylinder-like micelles which are connected 3-by-3 to construct the Cub phases in the longer chain members. The formation of the *Im*3*m*-Cub phase is realized at the boundary of the two *Ia*3*d*-Cub phase regions.

Acknowledgment. We first thank Prof. Emeritus Michio Sorai at Osaka University and Prof. Keiichi Moriya at Gifu University for stimulating discussions and encouragement. Prof. Yuji Naruse at Gifu University helped us calculate the molecular structure. We also thank Prof. Shuichi Nojima at Tokyo Institute of Technology and Mr. Shouhei Shimizu and Mr. Takeya Ito at Gifu University for their various experimental aids. This work was partly supported by a Grant-in-Aid for Scientific Research (C) 18550121 from the Japan Society for the Promotion of Science and by a Grant-in-Aid for Scientific Research on Priority Areas (446/19022012) from the Ministry of Education, Culture, Sports, Science and Technology (MEXT) (both for S.K.), and by a Grant-in-Aid for Scientific Research on Priority Areas (463/19031002) from MEXT (K.S.). Beam time at PF-KEK provided by Programs 2004G297 and 2006G342 is also acknowledged.

Supporting Information Available: Techniques and instruments, and synthetic procedures and analytical data of all compounds, including Figures S0−S16 and Tables S1 and S2 (PDF). This material is available free of charge via the Internet at http://pubs.acs.org.

CM703684V

(57) Strictly speaking, the two alkyl chains might be obliquely directed with respect to the long axis of the core part, especially in the SmC phase, and thus the molecules would have somewhat of a zig-zag shape. In this discussion, however, we ignore this fact and regard the molecular shape as being rodlike, if the alkyl and hydrogen-bonding effects are equally balanced. Also, in Figure 12, only a half of the molecule is schematically depicted for clarity.